



**HAL**  
open science

## Experimental procedure and results to measure the composition of gas hydrate, during crystallization and at equilibrium, from N<sub>2</sub>-CO<sub>2</sub>- CH<sub>4</sub>-C<sub>2</sub>H<sub>6</sub>-C<sub>3</sub>H<sub>8</sub>-C<sub>4</sub>H<sub>10</sub> gas mixtures

Duyen Le Quang, Du Le Quang, Baptiste Bouillot, Jean-Michel Herri, Philippe Glénat, Pierre Duchet-Suchaux

### ► To cite this version:

Duyen Le Quang, Du Le Quang, Baptiste Bouillot, Jean-Michel Herri, Philippe Glénat, et al.. Experimental procedure and results to measure the composition of gas hydrate, during crystallization and at equilibrium, from N<sub>2</sub>-CO<sub>2</sub>- CH<sub>4</sub>-C<sub>2</sub>H<sub>6</sub>-C<sub>3</sub>H<sub>8</sub>-C<sub>4</sub>H<sub>10</sub> gas mixtures. *Fluid Phase Equilibria*, 2016, 413, pp.10-21. 10.1016/j.fluid.2015.10.022 . hal-01220228

**HAL Id: hal-01220228**

**<https://hal.science/hal-01220228>**

Submitted on 22 Aug 2016

**HAL** is a multi-disciplinary open access archive for the deposit and dissemination of scientific research documents, whether they are published or not. The documents may come from teaching and research institutions in France or abroad, or from public or private research centers.

L'archive ouverte pluridisciplinaire **HAL**, est destinée au dépôt et à la diffusion de documents scientifiques de niveau recherche, publiés ou non, émanant des établissements d'enseignement et de recherche français ou étrangers, des laboratoires publics ou privés.

**EXPERIMENTAL PROCEDURE AND RESULTS TO MEASURE THE COMPOSITION  
OF GAS HYDRATE, DURING CRYSTALLIZATION AND AT EQUILIBRIUM, FROM  
N<sub>2</sub>-CO<sub>2</sub>- CH<sub>4</sub>-C<sub>2</sub>H<sub>6</sub>-C<sub>3</sub>H<sub>8</sub>-C<sub>4</sub>H<sub>10</sub> GAS MIXTURES**

**LE QUANG Duyen, LE QUANG Du, \*BOUILLOT Baptiste, HERRI Jean-Michel**  
Gas Hydrate Dynamics Centre, Ecole Nationale Supérieure des Mines de Saint-Etienne,  
Centre SPIN - LGF UMR CNRS 5307  
158 Cours Fauriel, 42023 Saint-Etienne, France,

**GLENAT, Philippe,**  
TOTAL S.A., CSTJF, Avenue Larribau, 64018 PAU Cedex, France

**DUCHET-SUCHAUX, Pierre**  
TOTAL S.A., 2 place Jean Millier La Défense 6 92400 Courbevoie, France

**ABSTRACT**

Mixed Clathrate hydrates are an important issue in many fields, like flow assurance in the oil industry, as well as gas capture and storage, air conditioning, etc...

Usually, studies of gas hydrates from hydrocarbon gas mixtures do not mention the volume of hydrate, nor the hydrate composition, and ternary or quaternary mixtures are not considered. Also, data involving propane and butane are limited.

Therefore, we suggest both an experimental and modeling study of mixed clathrate hydrates from N<sub>2</sub>-CO<sub>2</sub>-CH<sub>4</sub>-C<sub>2</sub>H<sub>6</sub>-C<sub>3</sub>H<sub>8</sub>-C<sub>4</sub>H<sub>10</sub> gas mixtures, in temperature range of [0.8-19°C] and pressure range of [1.4 – 66bars]. The experimental work provides 78 equilibrium points. Two procedures were used to perform crystallizations. The main procedure (71 equilibrium data) corresponds to a method at high crystallization rate (high supersaturation, or high ΔP). The first objective is to study the gas hydrates formation in usual dynamic conditions (start-up or reboot of an oil exploitation). The second method, 7 data, corresponds to a low rate of crystallization. This second objective is to investigate the impact of the speed of crystallization on the final equilibrium. For both procedures, P-T data are given, as well as the compositions of each phase at equilibrium.

At last, thermodynamic modeling is used to compare the experimental results of both procedures. Kihara parameters of N<sub>2</sub>, CO<sub>2</sub> and CH<sub>4</sub> are taken from the literature, while parameters for C<sub>2</sub>H<sub>6</sub> are regressed and given in this work.

Results show a better agreement of the thermodynamic modeling with experimental study for pure gas hydrate and mixed gas hydrates at low crystallization rate. This observation suggests that mixed gas hydrates might form at thermodynamic equilibrium only at low crystallization rate.

*Keywords:* Clathrate hydrates, Experimental study, Thermodynamics, Phase equilibria

*\* To whom correspondence should be addressed: bouillot@emse.fr*

## 1. Introduction

Gas hydrates, or clathrate hydrates, are components crucial components in many fields. Flow assurance issue is probably the reason why they were so widely studied in the past decades [1]. Exploration and exploitation of methane hydrate buried in permafrost and deep-sea is also a major issue [2], as well as gas capture and storage (mainly CO<sub>2</sub>) [3].

Pipe-line plugging in the oil industry is the start of the study, brought by TOTAL SA about hydrocarbon gas mixtures. Indeed, the interest for unconventional oil resources is growing (mainly in deep-offshore). In this situation, hydrate risk is significant and has to be controlled (zero tolerance policy).

Therefore, to study the hydrate risk of formation, experimental data as well as thermodynamic modeling, are essential. But, if gas hydrate from hydrocarbon gas mixtures has been widely studied, few data involving propane and butane are available. Moreover, these studies do not provide the hydrate volume and water consumption. Sometimes, a modelling approach is suggested using classic van der Waals and Platteuw theory [4]. The use of such theory usually involves parameters, the so-called Kihara parameters. However, these parameters are very dependent on the authors and on the quality of the experimental data used (both equilibrium data and reference thermodynamic properties). We showed in a previous paper such differences ( $\epsilon/k$  from 165 to 175 for CO<sub>2</sub> as example) [5]. This is why acquiring accurate and complete data is an essential part of the modeling work. But, obtaining satisfying results can be tricky if hydrate crystallization involve kinetic considerations.

In this work, gas hydrates from CO<sub>2</sub>-CH<sub>4</sub>-C<sub>2</sub>H<sub>6</sub>-C<sub>3</sub>H<sub>8</sub>-C<sub>4</sub>H<sub>10</sub> gas mixtures are studied. To go further in the experimental approach, the procedure used provides not only the measurement of the classic Pressure/Temperature data at equilibrium, but also the hydrate composition and volume.

To evaluate the influence of the speed of crystallization on the final state, two procedures were used: at high crystallization rate (high driving force, for example at the start-up of a well), and at low crystallization rate (low driving force, corresponding to steady state exploitation). 12 Experiments were performed providing 78 equilibrium points. 71 data were obtained from quick crystallization, and 7 from slow crystallization experiments.

In the end, experimental results were compared to the classic van der Waals and Platteuw model. Ethane Kihara parameters needed to be calculated. Parameters of propane and butane could not be regressed from pure gas hydrates.

## 2. Gas Hydrates

Gas hydrates, or clathrate hydrates, are ice-like crystalline compounds composed of molecules of water and small molecules (usually gaseous at standard conditions). They present different polymorphic structures depending on the guest molecules. Three main structures were identified: SI, SII and SH ([6]). Table I presents a brief description of classic clathrate hydrate structures.

These compounds may be formed at low temperature and high pressure. The liquid-hydrate phase diagrams depend on the structure (I, II, H) and guest molecules, see figure 2 as example.

## 3. Materials and methods

### 3.1 Experimental set-up

The experimental set-up (figure 2) allows the measure of hydrate equilibria. From temperature and pressure measurements, as well as gas and liquid sampling, the equilibrium state can be completely determined: compositions and masses of each phase in the reactor. The apparatus composed of an instrumented batch reactor (Autoclave, 2.36 L). This reactor is fed with pure gas, or prepared gas mixture. A HPLC pump (JASCO-PU-1587) is used to inject the liquid phase (water + LiNO<sub>3</sub>, used as tracer for the determination of the water concentration). A cryostat (HUBERT CC-505) keep a constant temperature in the reactor (0.02°C accuracy), and two sapphire windows (12cm x 2cm) are placed on each sides of the reactor to keep an eye on the crystallization. The reactor is stirred on the upper side (vapor phase) and lower side (liquid/hydrate

phase). The pressure, as well as the temperature on the upper/lower side, is monitored online with a data acquisition system (Pt 100, accuracy 0.02°C, pressure accuracy 0.1 bar).

To determine the composition of each phase at equilibrium (by mass balance calculations), the gas phase composition is sampled (ROLSI™) and injected in a gas chromatograph (VARIAN model CP-3800 GC with a 50m PORA BOND Q column). A few  $\mu\text{m}^3$  is taken each time. Helium is used a carrier gas in the GC. The liquid phase is analyzed offline by ionic chromatography (DIONEX ionic exchange chromatograph). A simple valve is used to sample the liquid phase (water +  $\text{LiNO}_3$ ).

### 3.2 Experimental procedure at high crystallization rate

The first experimental procedure is the same as in previous studies [5]. Figure 3 shows the crystallization and dissociation process. This procedure is performed at high crystallization rate (or at a high supersaturation). For gas hydrates this means high  $\Delta P$  (or high  $\Delta T$ ).

At the beginning, the reactor is cleaned and emptied (40 minutes). Then, the cell is filled with gas mixture, either by direct injection of the pure gases or from a prepared bottle.

The pressure is measured, and the temperature is then set to 0-1°C (internal regulation of the cryostat). The gas composition in the cell is checked with GC analysis at the beginning and before any measurement.

A 10 mL/L water mixture of  $\text{LiNO}_3$  is prepared and injected (about 800g) into the reactor thanks to a HPLC pump (n°13). Ultrapure water is used (first category, 18.2 M $\Omega$ .cm). The  $\text{LiNO}_3$  is added as a tracer to measure the water concentration, and thus the volume. A pressure rise, due to the added volume of liquid, is observed. Then, the reactor is stirred at 450 rpm rate, on the upper and bottom side of the reactor. The gas is dissolved into the liquid phase. After a while (induction time), the crystallization begins. Due to the exothermicity of the reaction, a brief raise of temperature is observed. At this point, we wait for the equilibrium to happen (stabilization of temperature and pressure). This takes about 2 to 4 days depending on gas mixture and initial pressure. When the equilibrium is reached, a sample of the gas phase is taken and injected into the gas chromatograph to determine the molar composition. A liquid sample is also taken to be analyzed *offline* by ionic chromatography (about 4.5mg).

At this moment, the dissociation of the hydrate start. The temperature is increased of 1.5°C. When the new equilibrium is reached (about 24h), new samples of the fluid phases are taken. Then, the process is repeated until there is no more hydrates into the reactor. The whole procedure is summarized on figure 3. This concerns gas mixtures n°1 to n°11 in table 2.

### 3.3 Experimental procedure at low crystallization rate

The objective of this second procedure is to focus on thermodynamic equilibrium, limiting as much as possible kinetic effects. In this case, the crystallization rate is closer to hydrate formation in pipelines at steady state (constant and low evolution of the pressure and temperature).

Only the last experiment (n°12, see table 2) is concerned. The aim is to investigate and give perspectives for mixed hydrates equilibrium modeling (thermodynamics or kinetics?).

Figure 4 illustrates this method. Instead of decreasing very quickly the temperature to the final state (between 0 and 2°C), the crystallization occurs close to the first liquid-hydrate equilibrium temperature. Then, the temperature is decreased very slowly (about 0.1 to 0.2 °C per day). Every 1°C decreased, samples of both gas and liquid phases are taken and analyzed.

### 3.4 Gas compositions

Studied gas compositions are given in table 2. There are 12 gas mixtures from  $\text{N}_2$ - $\text{CO}_2$ - $\text{CH}_4$ - $\text{C}_2\text{H}_6$ - $\text{C}_3\text{H}_8$ -(n- $\text{C}_4\text{H}_{10}$ ). Gases were provided by Air Liquid and Air Product ( $\text{CO}_2$  premium, impurities < 60ppm, nitrogen premium impurities < 6ppm, methane 3.5, ethane 2.5, propane 3.5 and n-butane 3.5). These initial compositions given in table 2 were determined by GC (n°9 on figure 2).

To prepare these gas mixtures, two methods were applied: For binary mixtures (gas 3 to 5), the mixtures were prepared from pure gas directly connected to the reactor. The less volatile gas (CO<sub>2</sub>) was first injected into the reactor. Then, the second one (N<sub>2</sub> or CH<sub>4</sub>) was injected. The knowledge of the pressure after each injection, and the use of the Soave-Redlich-Kwong (SRK) equation of state, allow the calculation of the number of mole of each gas (and so the gas composition).

The second method used was a prior preparation of the mixtures. Bottles were prepared by injecting the different pure gases, from the less volatile to the most volatile, and by weighting the bottle after each injection. Molar composition was calculated from the knowledge of the injected mass of each gas. To homogenize the mixtures, bottles were not used before a few days after the preparation.

A 20% margin from the vapor pressure was chosen in order to avoid any condensation in the gas cylinders and in the reactor.

### 3.5 Phase Compositions

#### 3.5.1 Mass balance

The calculation of the composition of each phase (superscripts  $G$ ,  $L$ , and  $H$  for respectively the gas, the aqueous phase and the hydrate) is a standard mass balance for each component  $j$  based on the experimental measurements (Li<sup>+</sup> concentration in the aqueous phase, pressure, temperature and gas composition):

$$n_j^0 = n_j^G + n_j^L + n_j^H \quad (1)$$

#### 3.5.2 Gas phase calculation

The gas phase density (initial gas mixture, superscript <sup>0</sup>, and at equilibrium) is calculated by the following equation:

$$PV = Z(P, T, z)n^G RT \quad (2)$$

The compressibility factor  $Z$  is calculated using SRK Equation of State which. This equation is of reasonable accuracy for the moderate pressures and gases used in these experiments [10]. The SRK parameters used are given in table 3.

The gas composition  $z$  in the SRK equation is experimentally measured by GC. The initial volume of the gas  $V^0$  is the volume of the reactor,  $V_R$  (=2.36 L). The gas volume at the equilibrium is:

$$V^G = V_R - V^L - V^H \quad (3)$$

The two last volumes are calculated thanks to the knowledge of the water concentration (see 3.5.3). In the end, the SRK EoS allows the calculation of  $n_j^0$  and  $n_j^G$ .

#### 3.5.3 Liquid phase calculation

The liquid phase calculation is a three steps calculation:

- Calculation of the water mass (or volume) in the liquid phase,
- Calculation of the hydrates volume (water mass balance).
- Calculation of the vapor-liquid equilibrium.

Liquid volume is calculated with the LiNO<sub>3</sub> concentration (added as tracer). This tracer is not involved in the crystallization process, and the quantity of each ion remains constant in the aqueous phase. From the Li<sup>+</sup> concentration (obtained by ionic chromatography), the liquid volume is deduced (conservation of Li<sup>+</sup> ions quantity):

$$V^L = \frac{V_0^L [Li^+]_0}{[Li^+]} \quad (4)$$

Equation (4) gives the water mass in the liquid phase, as well as the mass of water in the hydrate phase (mass balance). Note: we neglect the water in the gas phase. Knowing the mass of water in the hydrate phase, the hydrate volume is calculated from theoretical empty hydrate structure density. This density is obtained from lattice constants [6], and depends on the structure (790kg/m<sup>3</sup> for SI structure, and 785kg/m<sup>3</sup> for SII structure).

Then, the number of moles of gas molecules in the liquid phase is calculated with the use of Henry's law. The vapor-liquid equation used is the following one:

$$n_j^L = \frac{V^L \rho_w^0 z_j \varphi_j^G P}{M_w K_{H,j}^\infty} \quad (5)$$

Some assumptions are made: the fugacity coefficients in the gas phase  $\varphi_j^G$  are taken equal to the unity. The Poynting correction is neglected. The water density is considered to be 1000 kg/m<sup>3</sup>. The Henry's constants  $K_{H,j}^\infty$  are calculated using Holder correlation [11]:

$$K_{H,j}^\infty(T) = \exp\left(A + \frac{B}{T}\right) \quad (6)$$

The A and B constants are given in table 4.

In the end, equation (4) allows the calculation of  $n_j^L$ .

### 3.5.4 Hydrate phase calculation

The hydrate phase calculation comes from a mass balance on the hydrocarbons components (equation 1). The hydration number is also calculated.

### 3.6 Sampling effects and uncertainties

The gas sampling is assumed to be negligible (a few  $\mu\text{m}^3$  per sample). But the masses of water and Li<sup>+</sup> ions are taken into account in the calculation: the mass of water in the reactor is actualized at each step, as well as the new  $[Li^+]^0$  concentration. This variation is due to the liquid sampling (about 4-5mL per sample).

Evaluation of the various sources of errors in the calculations was made and described previously [5]. This evaluation led to an uncertainty on the gas phase  $\Delta z_i < 10^{-3}$  (determined from GC errors), and to an uncertainty of the hydrate phase of  $\Delta x_i/x_i < 6\%$ . In the present work, another evaluation was performed using Monte Carlo simulations using the following assumptions:

- $\Delta[Li^+]/[Li^+] = 0.1\%$ ,
- $\Delta z_i \approx 10^{-3}$ ,
- $\Delta T = 0.2^\circ\text{C}$ ,
- $\Delta P = 0.1 \text{ bar}$ ,
- $\Delta m_w = 0.1\text{g}$ ,
- $\Delta V_R = 3\%$ ,
- $\Delta \rho_w = 10 \text{ kg.m}^{-3}$ ,

- $\Delta \rho_H^\beta = 40 \text{ kg.m}^{-3}$ .
- $\rho_{\text{water}} = 1000 \text{ kg/m}^3$ .
- $\rho_H^\beta = 790 \text{ kg/m}^3$  (structure I from lattice constant [6])

Monte Carlo simulations were performed 1000 times (each point). The molar fraction errors on the hydrate composition of major molecules were found to be lower than 4%. The minor molecules ( $z_i < 5\%$ ) present uncertainties from 4% to 50%. The standard deviations close to the total dissociation point were calculated to be between 20% and 100%. Indeed, the initial and final  $\text{Li}^+$  concentrations for these points are very close. In any case, the obtained deviations are higher than the previous evaluation [5].

In the result tables, we chose to give the maximum absolute deviation, instead of giving the relative deviation. The Monte Carlo simulations provided a maximum absolute deviation of  $3.10^{-3}$  concerning the hydrate composition (in molar fractions).

Note: since the hydrates amount is obtained by difference in water concentration, the more crystals there are, the more accurate are the calculations.

## 4. Theory of clathrate hydrate equilibrium

### 4.1. Thermodynamic modeling

Classic van der Waals and Platteuw model [4] was used for the description of the hydrate phase, leading to the standard Liquid-Hydrate equilibrium (LHE) equation:

$$\Delta\mu_w^{H-\beta} = \Delta\mu_w^{L-\beta} \quad (7)$$

Where  $\Delta\mu_w^{H-\beta}$  and  $\Delta\mu_w^{L-\beta}$  are the difference between the chemical potential of the water in the hydrate phase (respectively the liquid phase) and the chemical potential of the reference  $\beta$  phase (empty clathrate).  $\Delta\mu_w^{L-\beta}$  is described by classic thermodynamics (Gibbs-Duhem equation) while  $\Delta\mu_w^{H-\beta}$  is expressed from statistical thermodynamics:

$$\Delta\mu_w^{H-\beta} = RT \sum_i v_i \ln(1 - \sum_j \theta_j^i) \quad (8)$$

#### 4.1.1 Hydrate phase

In equation (8),  $v_i$  is the numbers of cavities of type  $i$ , and  $\theta_j^i$  is the occupancy factor of molecule  $j$  in the cavity  $i$ . This parameter is the most important to define the thermodynamic equilibrium and the hydrate properties.

Usually, this last term is described by a model based on Langmuir adsorption theory [12]:

- The guest molecule is adsorbed at the surface,
- The adsorption energy is independent from the presence of other adsorbed molecules,
- The maximum amount of adsorbed gas corresponds to one molecule per site (one molecule par cavity),
- The expression of the occupancy factor  $\theta_j^i$  is given by:

$$\theta_j^i = \frac{c_j^i f_j(T,P)}{1 + \sum_j c_j^i f_j(T,P)} \quad (9)$$

Leading to:

$$\Delta\mu_w^{H-\beta} = RT \sum_i v_i \ln(1 - \sum_j C_j^i f_j(T, P)) \quad (10)$$

Where  $C_j^i$  is the Langmuir constant of component  $j$  in the cavity  $i$ . It describes the interaction potential between the encaged guest molecule and the surrounding water molecules of the spherically symmetrical cavity.  $C_j^i$  is expressed from a spherical symmetrical potential:

$$C_j^i = \frac{4\pi}{kT} \int_0^{R-a} \exp\left(-\frac{\omega(r)}{kT}\right) r^2 dr \quad (11)$$

where  $\omega(r)$  is the interaction potential between the cavity and the guest gas molecule according to the distance  $r$ .  $(R-a)$  is the difference between the cavity radius and the molecule radius. It means that the only interactions between guest molecules and the surrounding water molecules of the cavity are taken into account. This is a commonly accepted simplification.

Interaction potential  $\omega$  can be calculated using different models. The most commonly used for this purpose is the Kihara potential [13]:

$$\omega(r) = 2Z\varepsilon \left[ \frac{\sigma^{12}}{R^{11}r} \left( \delta^{10} + \frac{a}{R} \delta^{11} \right) - \frac{\sigma^6}{R^5 r} \left( \delta^4 + \frac{a}{R} \delta^5 \right) \right] \quad (12)$$

with:

$$\delta^N = \frac{1}{N} \left[ \left( 1 - \frac{r}{R} + \frac{a}{R} \right)^{-N} - \left( 1 + \frac{r}{R} + \frac{a}{R} \right)^{-N} \right] \quad (13)$$

The parameters  $\varepsilon$ ,  $\sigma$  and  $a$  are the so-called Kihara parameters. They are molecule dependent, and fitted from experimental results. Hence, they are characteristics of the guest molecules. The parameter  $\varepsilon$  stands for the maximum attractive potential; the parameter  $\sigma$  represents the distance from the cavity center at which the interaction potential is zero. At last,  $a$  is the spherical hard-core radius. It is a geometric parameter.

In the case of gas hydrates, only  $\varepsilon$  and  $\sigma$  are considered as fitting parameters. Since  $a$  is a geometric parameter, its value is known and set once for all. To fit these parameters, P-T equilibrium data from pure gas phase are needed. If this is not sufficient, the use of data from gas mixtures is a good complement, provided that the equilibrium composition of the hydrate phase is known, and that the results are at thermodynamic equilibrium. This last remark can be critical. More details on the Kihara parameters optimization can be found in Herri et al., 2011[5], and in section 4.2.

#### 4.1.2 Liquid phase

Chemical potential of the liquid phase can be written:

$$\Delta\mu_w^{L-\beta} = T \frac{\Delta\mu_w^{L-\beta}|_{T^0, P^0}}{T^0} + \left( b_{p,w}^{L-\beta} T^0 - \Delta c_{p,w}^{L-\beta}|_{T^0, P^0} \right) T \ln \frac{T}{T^0} + \frac{1}{2} b_{p,w}^{L-\beta} T (T^0 - T) + \left( \Delta h_w^{L-\beta}|_{T^0, P^0} + \left( b_{p,w}^{L-\beta} T^0 - \Delta c_{p,w}^{L-\beta}|_{T^0, P^0} \right) T^0 - \frac{1}{2} b_{p,w}^{L-\beta} T^0 \right) \left( 1 - \frac{T}{T^0} \right) + \Delta v_w^{L-\beta}|_{T^0} (P - P^0) - RT \ln x_w \quad (14)$$



$\Delta\mu_w^{L-\beta}$ ,  $\Delta h_w^{L-\beta}$ , and  $\Delta v_w^{L-\beta}$  are thermodynamic properties of the water liquid phase compared to the reference  $\beta$  phase (gas free hydrate structure). They are first order parameters.  $\Delta c_{p,w}^{L-\beta}|_{T^0,P^0}$  and  $b_{p,w}^{L-\beta}$ , secondary parameters, have been calculated by Sloan et al. [6] (see table 6).

Parameters  $\Delta\mu_w^{L-\beta}$  and  $\Delta h_w^{L-\beta}$  from Handa and Tse, 1986 [14] were used (see table 5).

More details on equation (14) can be found elsewhere [5]

This thermodynamic modeling has been implemented in our in-house software GasHyDyn which calculates the hydrates composition from the pressure and gas composition. This software does not perform a flash calculation. It does not provide the hydrate volume.

#### 4.2 Modeling Kihara parameters: Theory

The optimization of the Kihara parameters of the gas molecules is based on equation (7). For a given set of Kihara parameters and a given molecule, this equation provides the equilibrium pressure ( $P_{calc}$ ) at which  $\Delta\mu_w^{H-\beta} = \Delta\mu_w^{L-\beta}$ . Kihara parameters optimization is the minimization of the following deviation function:

$$F(\varepsilon_j, \sigma_j) = \sum_{l=1}^N \left| \frac{P_{calc}}{P_{exp}} - 1 \right| \rightarrow \min \left( \text{resp. } F(\varepsilon_j, \sigma_j) = \left| \frac{T_{calc}}{T_{exp}} - 1 \right| \rightarrow \min \right) \quad (15)$$

The index  $l$  is a specific data over  $N$  experimental data set. The calculations can be based on the pressure ( $P_{calc}$ ) knowing the temperature, and vice versa.

The whole optimization process has been explained in a previous work [5]. In a few words, for a given molecule, an experimental data set of LHE is chosen. Among these data, the temperature range has to be as wide as possible. Also, the whole data set has to be consistent. Then, calculations of the objective function  $F(\varepsilon_j, \sigma_j)$  are performed for different values of  $(\varepsilon_j, \sigma_j)$ . A diagram showing  $F$  as a function of the Kihara parameters is drawn. The minimum, when it exists, gives the best parameters. This optimization does not always provide a satisfying result. Sometimes, the minimum of the  $F$  function is not obvious, and additional data are needed. Usually, these data are the mixed hydrate composition. But, this brings a crucial problem. If the thermodynamic model is compared to mixed gas hydrate composition, then the experimental data have to be at thermodynamic equilibrium. How to be sure that they are? Indeed, the thermodynamic modeling only provides the hydrate composition of the first nucleus for a given gas composition and temperature (or pressure). This is experimentally hard to achieve. Moreover, by crystallizing a significant volume of hydrate, the measured composition corresponds to an average composition. The hydrate phase is presumed to be not homogeneous. So, the hydrate composition is a consequence of the crystallization process, influenced by the speed of the involved phenomena. This is why we used only pure hydrate data to regress the parameters ( $N_2$ ,  $CO_2$ ,  $C_2H_6$ ). Sometimes this could not be done ( $C_3H_8$ ,  $C_4H_{10}$ ).

The Kihara parameters obtained in this study ( $C_2H_6$ ), as well as in previous studies ( $N_2$ ,  $CO_2$ ,  $CH_4$ ), are given in table 7. Next section quickly explains how these parameters were optimized.

#### 4.3 Modelling Kihara parameters of $N_2$ , $CO_2$ , and $CH_4$

Kihara parameters for  $N_2$ ,  $CO_2$ , and  $CH_4$  have been obtained from pure clathrate hydrates by assuming a SI structure in the work of Herri and Chassefière 2012 [15]. These parameters are used in the present work.

#### 4.4 Modelling Kihara parameters of ethane

The Kihara parameters have been obtained for pure ethane clathrate hydrate by assuming a SI structure. The equilibrium data are numerous (Figure 5) and 61 experimental results have been retained for the optimisation, from Yasuda and Ohmura (2008) [7], Robert et al. (1940) [16], Deaton and Frost (1946) [17], Reamer et al. (1952) [18], Falabella (1975) [19], Mohammadi and Richon (2010) [20], which covers a wide range of temperature from 200.08K to 287.4K and a pressure range from 8.3kPa to 3298kPa. On Figure 5, the deviation presents a clear minimum which can be considered as the best values of  $\varepsilon/k$  and  $\sigma$  (reported in Table 7).

Figure 6 shows the good correlation of GasHyDyn simulations to a wider range of experimental data from pure C<sub>2</sub>H<sub>6</sub> hydrates [7,16-26].

#### 4.5 Modelling Kihara parameters of propane and butane

Up, to now, the determination of the Kihara parameters for the propane has not been possible since no minimum was found from pure hydrates data. More data are needed, especially results giving the hydrate composition for binary mixtures.

The modeling of n-butane was not possible since very few data are available in the literature. Moreover, the optimization of the Kihara parameters is difficult because the vapor pressure of n-butane is quite low.

#### 4.6. Kinetic modeling

Mixed hydrate formation is suspected to occur at non-thermodynamic equilibrium. Kinetics could be predominant in the process. Herri and Kwaterski [27] suggested a new approach combining thermodynamic (for liquid water chemical potential) and kinetics (the expression of Langmuir constant in the hydrate chemical potential). This model leads to the calculation of the crystal growth rate and to different hydrate phase composition.

In the next sections, we investigate experimentally through the two procedures (quick and slow crystallization), LHE from hydrocarbon gas mixtures. A thermodynamic modeling follows these results.

## 5. RESULTS

### 5.1. Experimental Results

The experimental results are presented in tables 8, 9 and 10. Tables 8 and 9 correspond to the first procedure (high crystallization rate). Table 10 corresponds to the second procedure (low crystallization rate).

All these tables provide: the equilibrium pressure; temperature; gas phase composition; hydrate composition (except for Gas 6 and 7 that suffered from analysis problems); hydration number; water conversion (%mass); hydrate volume.

Pressure-Temperature results for mixed hydrates could not be compared to data from the literature since all authors studied different gas compositions. However, the results on pure gases can easily be compared. Figure 7 shows that the experimental results on pure CO<sub>2</sub> and pure CH<sub>4</sub> are in accordance with the literature. This is a satisfying observation. This shows that the obtained results, when they can be compared to other studies, are in accordance with them. Then, the calculated hydration numbers are usually between 5 and 10 (except the points close to total dissociation). This also is a good point. However, hydration numbers can be found higher than 8 due to uncertainties.

Results concerning mixed hydrates show a water conversion under 38% mass depending on the gas mixtures and the initial pressure, but are quite similar except for gas mixture n°12 (discussed later). The results also show that the selectivity of mixed gas hydrates to carbon dioxide, ethane and propane is good, compared to methane. Molar composition in the hydrate phase of the heaviest hydrocarbons is at least ten times higher than in the gas phase (mixtures 8 to 12). Uncertainties on the gas phase composition are usually lower than 4%.

The most interesting observation is the comparison between the two procedures (gas 1 to 11 compared to gas 12). Looking at gas 8 and 12, (with the “same” initial global composition), the PT data are a bit different (about 1.5°C at same equilibrium pressure). The equilibrium temperature is higher at low crystallization rate (for example at 35.6 bars and 37.75 bars). Moreover, the enclathration of C<sub>2</sub>H<sub>6</sub> is more important (mole fractions two times higher) while the molar fraction of CH<sub>4</sub> is lower. It shows that the enclathration of heavier molecules is larger at a slow process. Finally, the water conversion is slightly lower in the case of gas 12. This means that less hydrates were crystallized, and that there is a larger occupation of the cavities. These observations highlight the apparent kinetic effects on hydrate formation. In other words, the crystallization driving force affects the enclathration, of the guest molecules and hence their selectivity.

This statement can be supported by a modeling point of view, using thermodynamic models. In the next section, our in-house model is compared to the experimental results.

## 5.2. Modeling results and discussion

Standard LHE calculations (section 4) have been implemented in our in-house software, “GasHyDyn”. Tables 11 and 12 present the simulated results (predicted pressures and hydrate compositions) and the mean deviations to experimental results.

Concerning pure gases (mixtures 1 and 2), the simulations are very solid (mean deviations between 1.4% and 2.3%). This is not surprising since the Kihara parameter optimizations showed very good accordance to the experimental results on a wide range of temperature.

The case of mixed hydrate is more interesting. First, predicted equilibrium pressure for binary mixtures of CO<sub>2</sub>/N<sub>2</sub> or CO<sub>2</sub>/CH<sub>4</sub> are well predicted by the model (mean deviation between 2.4 and 3.2%). In these cases, the errors on the predicted hydrate compositions are between 10% and 30% for the major species and 50% for the minor species.

In the case of ternary mixtures, the mean deviations on the pressure and hydrate composition are higher. This means that it is more difficult to model LHE when more molecules are involved. Moreover, it is important to notice that the experimental hydrate composition is an average value. However, the results for ternary gas 12 (at low driving force) are in better accordance with the experimental data (than gases 7 and 8 at high rate). The mean deviation on the pressure is 1.8 assuming a S1 structure, and the molar composition errors are under 24%. From this observation, the crystallization of gas hydrates at low driving force (slow crystallization) is likely to occur at thermodynamic equilibrium. Maybe the hydrate crystal shows, in this case, are more homogeneous composition. At the contrary, formation at high driving force (quick crystallization) could involve kinetic considerations rather than thermodynamic.

Kinetics effects would not be a surprise. Indeed, the hydrate crystallization from an initial vapor-liquid equilibrium involves many transfer phenomena. First, the gas dissolution in the aqueous phase is usually a limiting step [29]. This is dependent on the driving force (fugacity difference), the contact surface and the mass transfer coefficients. Moreover, this affects the instantaneous gas concentration in the liquid phase, and so the driving force for the crystallization (LHE). Then, we suggested recently [27] that the enclathration of the gas molecules into the hydrate structure could be significantly affected by kinetics considerations (diffusion in the liquid hydrate layer). Depending on the rate of enclathration, and the crystal

growth speed, the final composition of the mixed hydrate could be different than predicted by thermodynamic modeling.

From the above results, the comparison of the experimental and modeling observations seems to confirm the influence of the crystallization rate. Unfortunately, equilibria involving propane and butane could not be simulated with the thermodynamic model. Indeed, the Kihara parameters could not be regressed. To give a new dimension to the thermodynamic modeling, and discuss more specifically the experimental results, a mass balance should be considered. This way, the hydrate volume could be compared with the simulation, and highlight more precisely the kinetic influence on the crystallization. This is the purpose of a parallel work [30].

## 6. Conclusion

Gas hydrates equilibrium experiments of hydrocarbon gas mixtures ( $\text{N}_2\text{-CO}_2\text{-CH}_4\text{-C}_2\text{H}_6\text{-C}_3\text{H}_8\text{-C}_4\text{H}_{10}$ ) were performed in an instrumented batch reactor. The molar compositions (gas phase and hydrate phase) were provided as well as the mass of each phase and liquid water consumption. Two procedures were used in order to investigate the importance of kinetics: quick and slow crystallization.

The results for pure gas hydrates are in very good accordance with literature data. Mixed gas hydrates could not be compared to literature results since few data are available with propane and butane. The experimental uncertainties on molar composition were usually lower than  $10^{-3}$  (absolute).

To evaluate the importance of kinetic effects on hydrate formation, a thermodynamic model, implementing classic van der Waals and Platteuw model, were used. The Kihara parameters used were taken from a previous study ( $\text{CH}_4$ ,  $\text{CO}_2$ ,  $\text{N}_2$ ) and calculated ( $\text{C}_2\text{H}_6$ ). They were obtained from pure gas hydrate equilibrium data (PT). Parameters for propane and butane could not be obtained.

The two procedures used suggest a kinetic influence on mixed hydrate formation. Experimental results showed that the enclathration of the heavier molecule (ethane) is more important at low than high crystallization rate. Moreover, the equilibrium pressure for a given temperature and initial gas composition, is slightly different. Finally, the thermodynamic simulations are also in better accordance with the results at slow crystallization.

In the end, the results show that mixed hydrate equilibrium could not be at thermodynamic equilibrium. If the measurements are performed at high crystallization rate the hydrate volume and composition will not be in accordance with the thermodynamic modeling. This observation could have a significant impact on design calculations in which the assumption of thermodynamic equilibrium is made (leading to an over estimation of the hydrates volume in the pipe-lines).

This is why the description of the procedure is essential. Authors have to be careful when computing and regressing model parameters if other data than PT are considered.

To extend the last discussion, a new approach of the modeling for the whole hydrate volume is presented in the same issue [30].

### List of symbols

- a Hard core radius [ $\text{\AA}$ ]
- $H$  Hydrate phase (as superscript)
- $j$  Molecule index (as subscript)
- k Boltzmann constant [ $\text{J/K}$ ]

$K_{H,j}^{\infty}$  Henry constant at solvent vapor pressure [Pa]  
 $L$  Liquid phase (as superscript)  
 $M_w$  water molecular weight [g/mol.]  
 $n_j^0$  Initial number of moles of molecule  $j$  [mol.]  
 $n_j^G$  Number of moles of  $j$  in the gas phase [mol.]  
 $n_j^L$  Number of moles of  $j$  in the liquid phase [mol.]  
 $n_j^H$  Number of moles of  $j$  in the hydrate [mol.]  
 $N_{\text{hyd}}$  Hydration number  
 $P$  Pressure [bar]  
 $r$  Distance between guest molecule and cavity [Å]  
 $R$  Cavity radius [Å]  
 $T$  Temperature [°C]  
 $x_j$  Mole fraction of  $j$  in the hydrate phase  
 $y_j$  Mole fraction of  $j$  in the liquid phase  
 $V$  Volume [m<sup>3</sup>]  
 $V^H$  Hydrate Volume [m<sup>3</sup>]  
 $V^L$  Liquid Volume [m<sup>3</sup>]  
 $V_R$  Volume of the reactor [m<sup>3</sup>]  
 $w$  Water (as subscript)  
 $z_j$  Mole fraction of  $j$  in the vapor phase  
 $\varepsilon$  maximum attractive potential [J]  
 $\rho_H^{\beta}$  Pure clathrate (gas free) density [kg.m<sup>-3</sup>]  
 $\rho_w$  Water density [kg.m<sup>-3</sup>]  
 $\sigma$  Soft core radius [Å]  
 $\varphi$  Fugacity coefficient  
 $\omega$  interaction potential [J]  
 $0$  initial situation (as subscript or superscript)

## Acknowledgements

The authors would like to thanks TOTAL SA for its support in this study.

The authors would also like to thanks all the members of the technical staff for their constant support: Alain Lallemand, Fabien Chauvy, Richard Drogo and Albert Boyer.

## References

- [1] E.D. Sloan, Fluid Phase Equilibria 228-229 (2008) 67-74.
- [2] T. Collett, J.J. Bahk, R. Baker, R. Boswell, D. Divins, M. Frye, D. Goldberg, J. Husebo, C.A. Koh, M. Malone, M. Morell, G. Myers, C. Shipp, M. Torres, J. Chem. Eng. Data 60(2) (2015) 319-329.
- [3] D. NguyenHong, F. Chauvy, J.M. Herri, Energy Conversion Manag. 48(4) (2007) 1313–1322.
- [4] J.H. Van der Waals, J.C. Platteeuw, Adv. Chem. Phys. 2 (1959) 1-57
- [5] J.M. Herri, A. Bouchemoua, M. Kwaterski, A. Fezoua, Y. Ouabbas, A. Cameirao, Fluid Phase Equilibria, 301 (2011) 171-190
- [6] E.D. Sloan, C.A. Koh, Clathrate hydrates of natural gases, 3rd ed., CRC Press, Boca Raton, 2007.
- [7] K. Yasuda, R. Ohmura, J. Chem. Eng. Data, 53 (2008) 2182-2188
- [8] S. Adisasmito, R.K. Frank, E.D. Sloan, J. Chem. Eng. Data, 36 (1991) 68-71
- [9] J.L. Thakore, G.D. Holder, Ind. Eng. Chem. Res. 26 (1987) 462.
- [10] A. Danesh, PVT and Phase Behavior of Petroleum Reservoir Fluids. Elsevier, 1998.
- [11] G.D. Holder, S.P. Zetts, N. Pradhan, N., Review in Chemical Engineering 5 (1988) 1-70.
- [12] V. McKoy, O.J. Sinanoğlu, J Chem. Phys 38 (1963) 2946-2956.
- [13] C.C. Chen, H.I. Britt, J.F. Boston, L.B. Evans, AIChE J., 28 (1982) 588-596.
- [14] Y.P. Handa, J.S. Tse, J. Phys. Chem. 23 (1986) 5917.

- [15] J.M. Herri, E. Chassefiere, *Planetary and Space Sciences* 73 (2012) 376-386.
- [16] O.L. Robert, E.R. Brownscombe, L.S. Howe, *Oil & Gas J.* 39(30) (1940) 37-43
- [17] W.M. Deaton, E.M. Frost, U.S., *Bur. Mines Monogr.*, 8 (1946) 1-101
- [18] H.H. Reamer, F.T. Selleck, B.H. Sage, *Trans. Am. Inst. Min., Metall. Pet. Eng.* 195 (1952) 197-202
- [19] B.J. Falabella, M. Vanpee, *Ind. Eng. Chem. Fundam.* 13 (1974) 228-231
- [20] A.H. Mohammadi, D. Richon, *Ind. Eng. Chem. Res.*, 48 (2010) 2976-3979
- [21] J. Jhaveri, D.B. Robinson, *Can. J. Chem. Eng.* 43 (1965) 75.
- [22] N. Fray, U. Marboeuf, O. Brissaud, B. Schmitt, *J. Chem. Eng. Data* 55(11) (2010) 5101-5108
- [23] D. Avlonitis, A. Danesh, A.C. Todd, *Master of Science Thesis*, Heriot-Watt University, Edinburgh, Cranfield, Uk, 1988
- [24] G.D. Holder, G.C. Grigoriou, *J. Chem. Therm.* 12(11) (1980) 1093-1104
- [25] G.D. Holder, J.H. Hand, *AIChE J.* 28(3) (1982) 440-447
- [26] T.J. Galloway, W. Ruska, P.S. Chapplelear, R. Kobayashi, *Ind. Eng. Chem. Fundam.* 9(2) (1970) 237-243
- [27] J.M. Herri, M. Kwaterski, *Chem. Eng. Sci.* 81 (2012) 28-37.
- [28] S.L. Miller, W.D. Smythe, *Science* 170 (1970) 531-533
- [29] J.M. Herri, F. Gruy, J.S. Pic, M. Cournil, *A.I.Ch.E. J.* 45(3) (1999) 590-602.
- [30] B. Bouillot, J.M. Herri, Submitted to *Fluid Phase Equilib.* (this issue).

## Figures

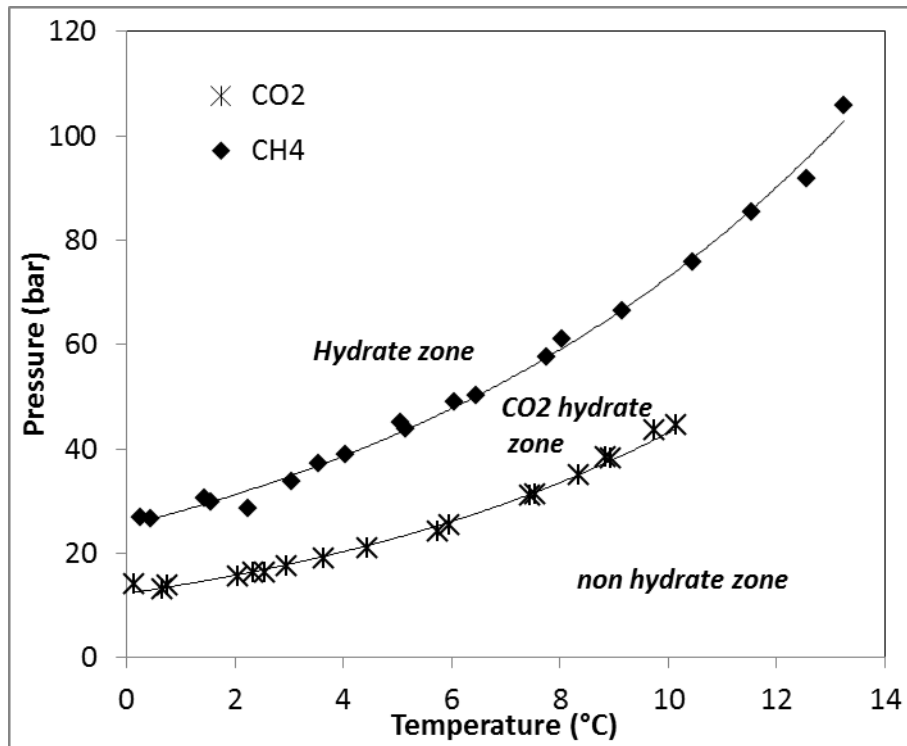


Figure 1. Experimental CO<sub>2</sub> and CH<sub>4</sub> P-T hydrate equilibria diagrams [7-9]

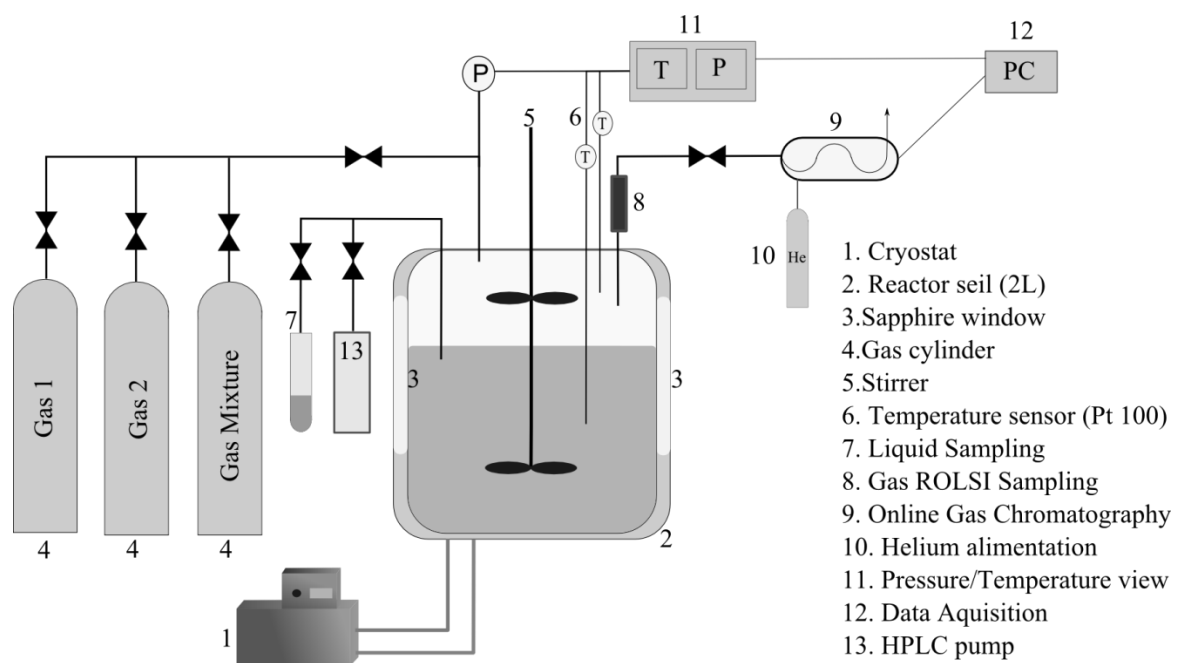


Figure 2. Experimental set-up



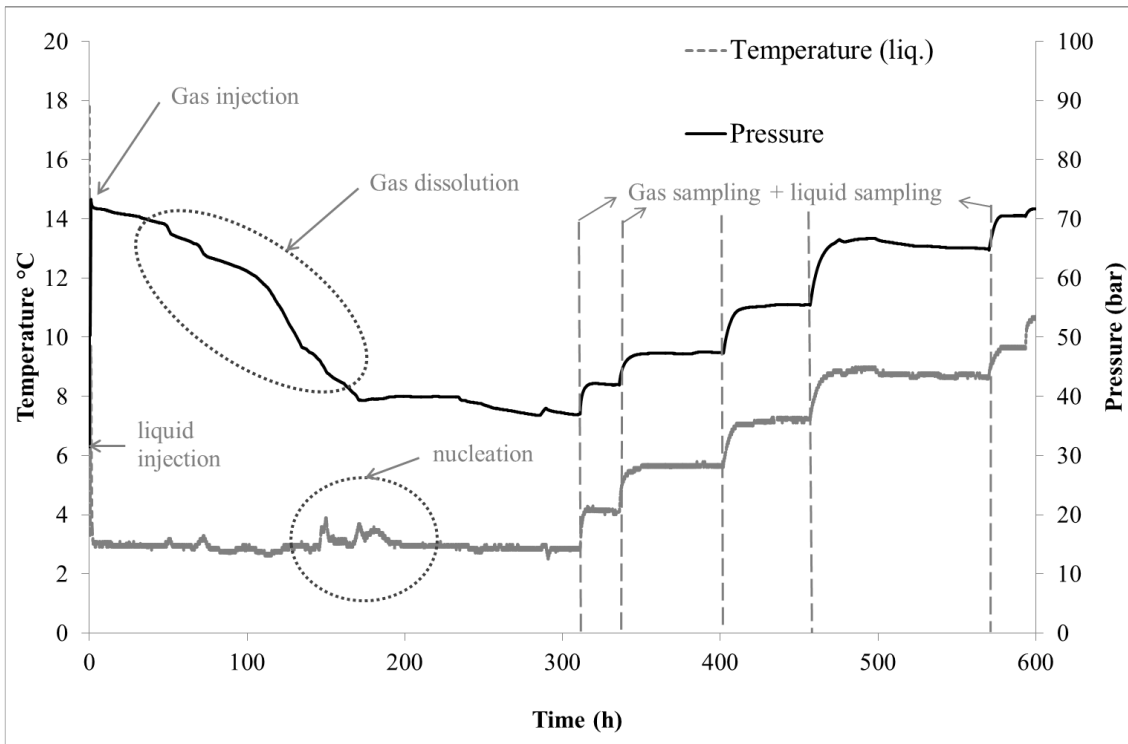


Figure 3. Pressure – Temperature evolution during equilibria experiments at high crystallization rate.

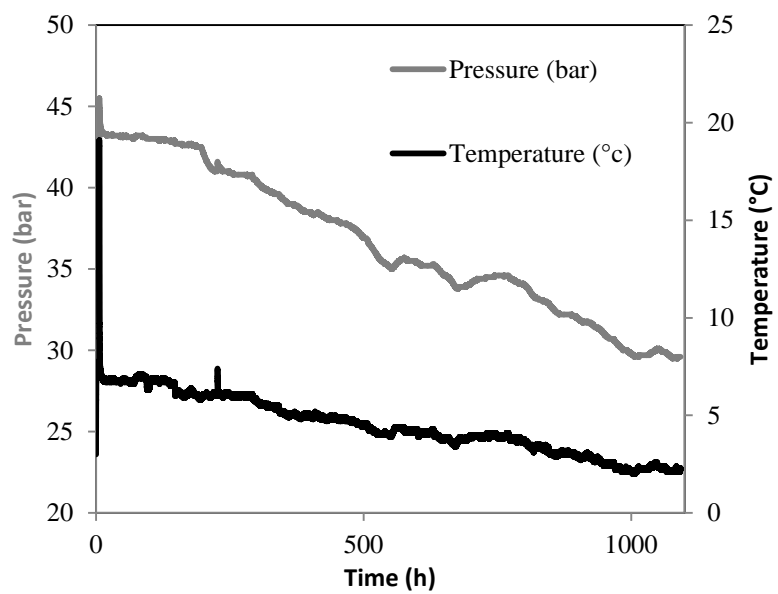


Figure 4. Pressure – Temperature evolution during equilibrium experiment at low crystallization rate.

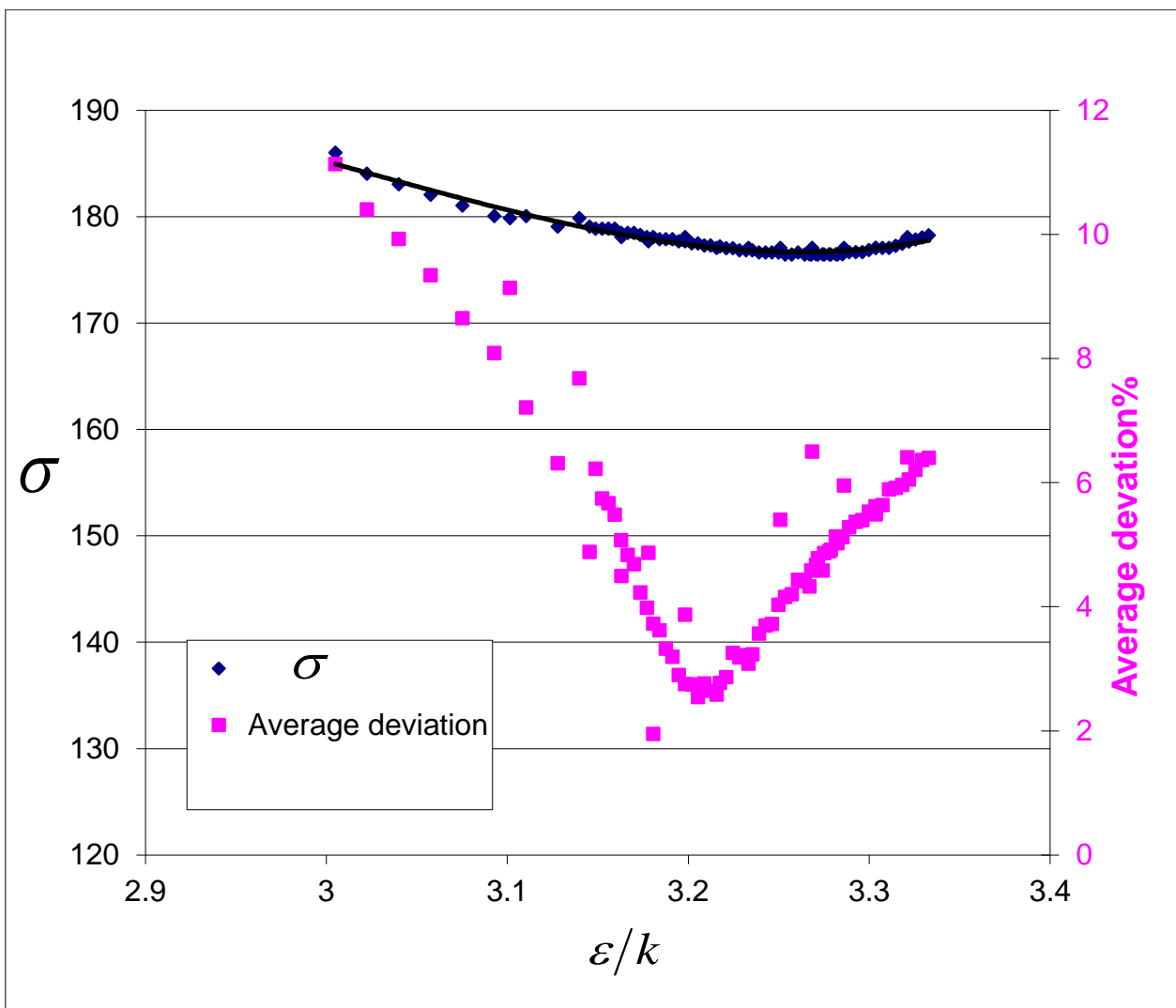


Figure 5.  $\epsilon/k$  versus  $\sigma$  at the minimum deviation with experimental data [7,16-20]. Pressure and temperature equilibrium data for  $C_2H_6$  hydrate over a wide range of temperature [200.08 - 287.4K] and pressure [8.3kPa - 3298kPa].

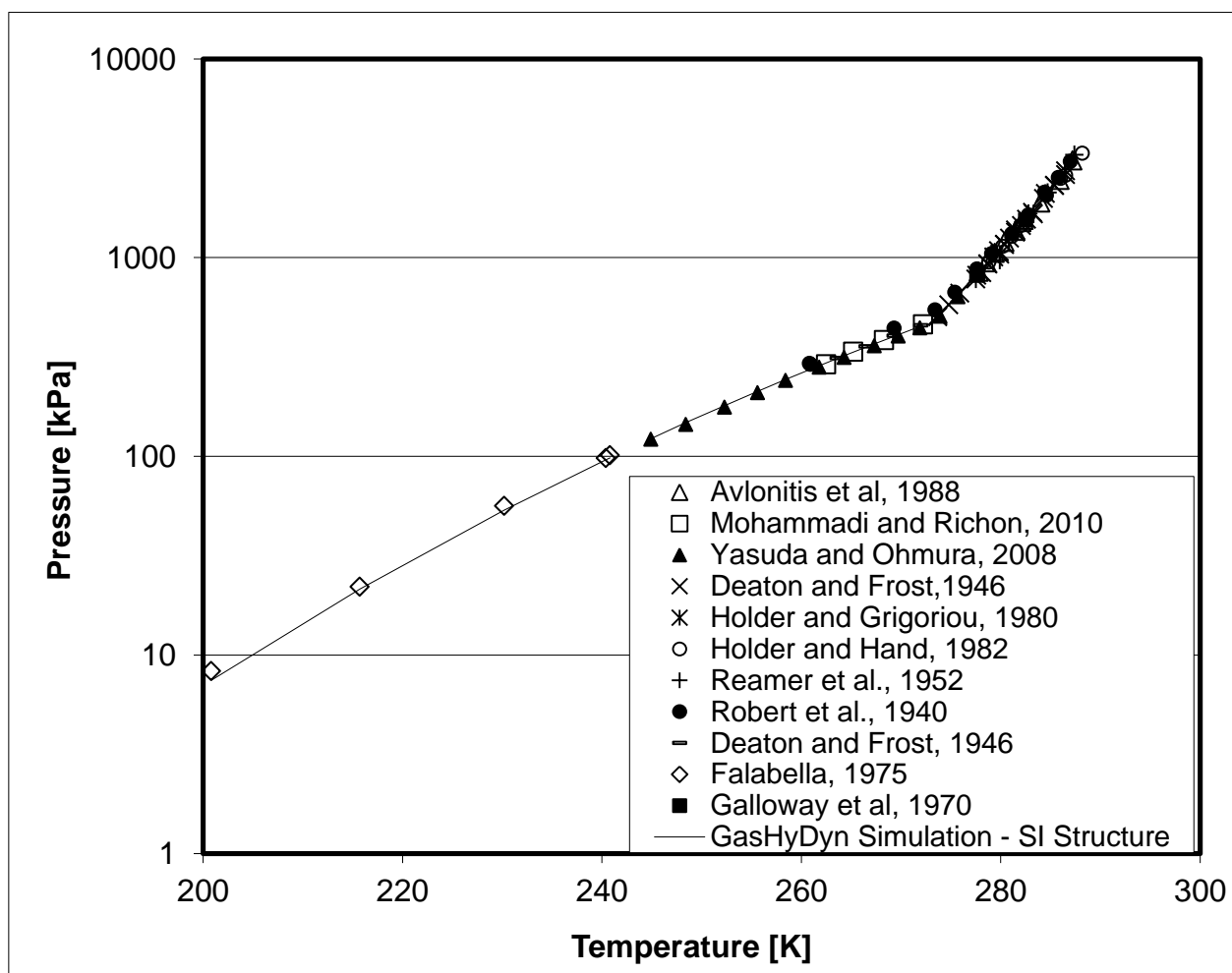


Figure 6. Hydrate-Liquid and Ice-Hydrate equilibrium of pure C<sub>2</sub>H<sub>6</sub>. The simulation curve is obtained with the GasHyDyn simulator assuming SI structure, implemented with reference parameters from Tables 5-6 and Kihara parameters given in Table 7

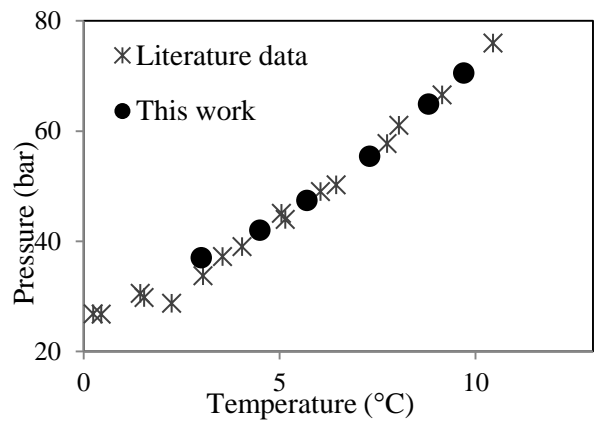
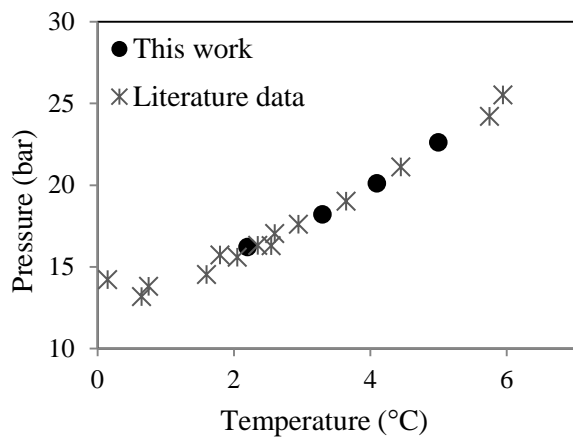


Figure 7. a) Experimental and literature [7-9] equilibrium data of pure CO<sub>2</sub> gas hydrates. b) for pure CH<sub>4</sub> gas hydrates [7-9, 17].

## Tables

Table 1. Structure of gas hydrates [6].

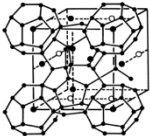
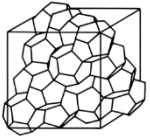
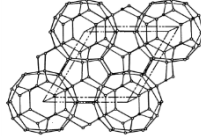
	<b>SI</b>		<b>SII</b>		<b>SH</b>		
							
<b>Cavity(*)</b>	$5^{12}$	$5^{12}6^2$	$5^{12}$	$5^{12}6^4$	$5^{12}$	$4^35^66^3$	$5^{12}6^8$
<b>Type of cavity</b>	<b>1</b>	<b>2</b>	<b>1</b>	<b>3</b>	<b>1</b>	<b>5</b>	<b>4</b>
<b>Number of cavity</b>	<b>2</b>	<b>6</b>	<b>16</b>	<b>8</b>	<b>3</b>	<b>2</b>	<b>1</b>
<b>Average cavity radius (nm)</b>	<b>0.395</b>	<b>0.433</b>	<b>0.391</b>	<b>0.473</b>	<b>0.391</b>	<b>0.406</b>	<b>0.571</b>
<b>Variation in radius,%</b>	<b>3.4</b>	<b>14.4</b>	<b>5.5</b>	<b>1.73</b>			

Table 2. Molar composition of studied gas mixtures (evaluated standard deviations about 0.001 abs. in mol. frac.) and initial conditions of experiments.

Gas mixtures	CO <sub>2</sub>	N <sub>2</sub>	CH <sub>4</sub>	C <sub>2</sub> H <sub>6</sub>	C <sub>3</sub> H <sub>8</sub>	n-C <sub>4</sub> H <sub>10</sub>	P <sub>i</sub> (bars ±0.1)	T <sub>i</sub> (K) (±0.2)	m <sub>w</sub> (±0.1 g)	V <sub>r</sub> (L) (±10 <sup>-3</sup> )
Gas 1	-	-	1	-	-	-	24.6	276.2	800.5	2.36
Gas 2	1	-	-	-	-	-	50.4	276.6	801.4	2.36
Gas 3	0.24	-	0.76	-	-	-	41.1	276.9	800.4	2.36
Gas 4	0.225	-	0.775	-	-	-	33.9	275.9	824.1	2.36
Gas 5	0.821	0.179	-	-	-	-	31.9	278.1	800.9	2.44
Gas 6	0.057	-	0.915	0.028	-	-	32.5	275.8	801.3	2.36
Gas 7	0.053	-	0.919	0.028	-	-	22	278.0	799.6	2.36
Gas 8	0.052	-	0.919	0.029	-	-	47.3	276.4	800.3	2.36
Gas 9	-	-	0.953	0.028	0.019	-	33.6	275.8	800.6	2.36
Gas 10	-	-	0.864	0.057	0.053	0.026	26.1	276.1	800.6	2.36
Gas 11	-	-	0.848	0.05	0.076	0.026	25.3	276.3	800.6	2.36
Gas 12	0.055	-	0.917	0.028	-	-	30.2	280.9	800.6	2.36

Table 3. SRK components parameters (from PRO/II<sup>®</sup> database).

$j$	T <sub>c</sub> (K)	P <sub>c</sub> (bar)	$\omega$	$k_{(N_2/j)}$	$k_{(CO_2/j)}$	$k_{(CH_4/j)}$	$k_{(C_2H_6/j)}$	$k_{(C_3H_8/j)}$	$k_{(C_4H_{10}/j)}$
N <sub>2</sub>	126.20	34.00	0.03772	0	-0.03	0.03	0.06	0.09	0.1130
CO <sub>2</sub>	304.21	73.83	0.22362	-0.03	0	0.0933	0.1363	0.1289	0.1430
CH <sub>4</sub>	190.56	45.99	0.01155	0.03	0.0933	0	-0.0078	0.009	0.0056
C <sub>2</sub> H <sub>6</sub>	305.32	48.72	0.09949	0.06	0.1363	-0.0078	0	0.0022	0.067
C <sub>3</sub> H <sub>8</sub>	369.83	42.48	0.15229	0.09	0.1289	0.009	-0.0022	0	-0.01
n- C <sub>4</sub> H <sub>10</sub>	425.15	37.99	0.2013	0.1130	0.1430	0.0056	0.067	-0.01	0



Table 4. Constants in equation (6) [11].

Gas	$A$	$B (K)$
CO <sub>2</sub>	14.283146	-2050.3269
N <sub>2</sub>	17.934347	-1933.381
CH <sub>4</sub>	15.826277	-1559.0631
C <sub>2</sub> H <sub>6</sub>	18.400368	-2410.4807
C <sub>3</sub> H <sub>8</sub>	20.958631	-3109.3918
n-C <sub>4</sub> H <sub>10</sub>	22.150557	-2739.7313

Table 5. Macroscopic parameters of hydrates and Ice [14]

<b>Structure I</b>		<b>Structure II</b>	
$\Delta\mu_w^{L-\beta}$	$\Delta h_w^{I-\beta}$	$\Delta\mu_w^{L-\beta}$	$\Delta h_w^{I-\beta}$
J/mol	J/mol	J/mol	J/mol
1287	931	1068	764

$\Delta h_w^{L-\beta,0} = \Delta h_w^{I-\beta,0} - 6011$ , where 6011 is the enthalpy of fusion of Ice (J/mol)

Table 6. Reference properties of hydrates from Sloan [6]

	Unit	Structure I	Structure II
$\Delta h_w^{L-\beta,0}$	J mol	$\Delta h_w^{I-\beta}  _{T^0,P^0,S_I} - 6011$	$\Delta h_w^{I-\beta}  _{T^0,P^0,S_{II}} - 6011$
$\Delta v_w^{L-\beta}  _{T^0}$	$10^{-6} \text{ m}^3/\text{mol}$	4.5959	4.99644
$\Delta c_{p,w}^{L-\beta}  _{T^0,P^0}$	J/(mol K <sup>-1</sup> )	-38.12	-38.12
$b_{p,w}^{L-\beta}$	J/(mol K <sup>-2</sup> )	0.141	0.141

Table 7.  $\varepsilon/k$  and  $\sigma$  parameters for N<sub>2</sub>, CO<sub>2</sub>, CH<sub>4</sub> [15] and C<sub>2</sub>H<sub>6</sub> (this work).  $a$  parameter from Sloan [6].

	$\varepsilon/k$	$\sigma$	$a$
CO <sub>2</sub>	178.21	2.873	0.6805
CH <sub>4</sub>	166.36	3.050	0.3834
N <sub>2</sub>	133.13	3.099	0.3526
C <sub>2</sub> H <sub>6</sub>	177.46	3.205	0.5651

Table 8. Experimental data (Gas 1 to 7)  
 \* equilibrium points near total dissociation, hydrate composition errors close to 100%  
 \*\* some composition data unavailable

Gas	P (±0.1 bar)	T (±0.2 °C)	Molar gas fraction (±0.001)					Molar hydrate fraction (±0.003)					Nhyd	water conversion % mass	Hydrate volume (mL ±4%)
			N <sub>2</sub>	CO <sub>2</sub>	CH <sub>4</sub>	C <sub>2</sub> H <sub>6</sub>	C <sub>3</sub> H <sub>8</sub>	N <sub>2</sub>	CO <sub>2</sub>	CH <sub>4</sub>	C <sub>2</sub> H <sub>6</sub>	C <sub>3</sub> H <sub>8</sub>			
1	16.2	2.2	-	1	-	-	-	-	1	-	-	-	5.58	-	-
	18.2	3.3	-	1	-	-	-	-	1	-	-	-	6.42	-	-
	20.1	4.1	-	1	-	-	-	-	1	-	-	-	7.28	-	-
	22.6	5	-	1	-	-	-	-	1	-	-	-	7.03	-	-
2	37	3	-	-	1	-	-	-	-	1	-	-	5.85	-	-
	42	4.5	-	-	1	-	-	-	-	1	-	-	6.56	-	-
	47.4	5.7	-	-	1	-	-	-	-	1	-	-	6.73	-	-
	55.4	7.3	-	-	1	-	-	-	-	1	-	-	6.57	-	-
	64.9	8.8	-	-	1	-	-	-	-	1	-	-	6.50	-	-
	70.5	9.7	-	-	1	-	-	-	-	1	-	-	2.81*	-	-
3	33.3	3.4	-	0.127	0.874	-	-	-	0.318	0.682	-	-	5.25	26.5	268.1
	35.3	4.4	-	0.134	0.866	-	-	-	0.319	0.681	-	-	5.8	27.2	274.2
	37.1	4.9	-	0.141	0.859	-	-	-	0.320	0.680	-	-	5.76	25.0	250.0
	40.3	5.8	-	0.151	0.849	-	-	-	0.320	0.680	-	-	5.93	21.8	216.4
	44.5	6.8	-	0.163	0.837	-	-	-	0.317	0.683	-	-	6.24	17.1	168.9
	49.3	7.8	-	0.175	0.825	-	-	-	0.296	0.704	-	-	6.21	9.79	96.1
	56	9	-	0.184*	0.817*	-	-	-	0.177*	0.823*	-	-	4.95	2.17	21.1
4	29.1	2.2	-	0.120	0.880	-	-	-	0.292	0.708	-	-	5.78	20.9	217.8
	29.7	2.5	-	0.129	0.871	-	-	-	0.282	0.718	-	-	6.59	23.3	241.2
	31.8	3.6	-	0.135	0.865	-	-	-	0.283	0.717	-	-	6.62	20.8	214.4
	34.7	4.5	-	0.147	0.853	-	-	-	0.270	0.730	-	-	7.11	18.3	187.2
	38	5.2	-	0.162	0.838	-	-	-	0.227	0.773	-	-	7.85	14.5	147.4
	41.6	6.4	-	0.177	0.823	-	-	-	0.101	0.899	-	-	9.98	10.6	106.8
	56.3	9.5	-	0.225*	0.775*	-	-	-	-*	-*	-	-	-*	-	-
5	24.6	2.46	0.333	0.667	-	-	-	0.059	0.941	-	-	-	6.25	22.4	226.6
	26	2.6	0.311	0.689	-	-	-	0.067	0.933	-	-	-	6.44	20.4	226.6
	26.6	2.66	0.301	0.699	-	-	-	0.073	0.927	-	-	-	6.63	19.9	206.8



Table 9. Experimental data (Gas 8 to 11)  
 \* equilibrium points near total dissociation, hydrate composition errors close to 100%  
 \*\* hydrate composition uncertainties  $\approx 10\%$  for  $C_2H_6$  and  $C_3H_8$

Gas	P ( $\pm 0.1$ bar)	T ( $\pm 0.2$ $^{\circ}C$ )	Molar gas fraction ( $\pm 0.001$ )					Molar hydrate fraction ( $\pm 0.003$ )					Nhyd	Water Conv. (%)	Hydrate Volume (mL $\pm 4\%$ )
			CO <sub>2</sub>	CH <sub>4</sub>	C <sub>2</sub> H <sub>6</sub>	C <sub>3</sub> H <sub>8</sub>	C <sub>4</sub> H <sub>10</sub>	CO <sub>2</sub>	CH <sub>4</sub>	C <sub>2</sub> H <sub>6</sub>	C <sub>3</sub> H <sub>8</sub>	C <sub>4</sub> H <sub>10</sub>			
8	35.4	2.75	0.025	0.964	0.011	-	-	0.070	0.888	0.042	-	-	5.16	34.1	345.3
	38.1	3.65	0.028	0.959	0.013	-	-	0.070	0.888	0.042	-	-	6.11	37.9	381.6
	42.3	5.15	0.031	0.952	0.017	-	-	0.069	0.891	0.041	-	-	6.27	34.2	342.2
	45.6	6.55	0.033	0.948	0.020	-	-	0.070	0.891	0.039	-	-	6.14	29.7	295.6
	51.2	7.8	0.035	0.943	0.021	-	-	0.068	0.889	0.042	-	-	6.20	23	227.6
	59.9	9.25	0.042	0.937	0.021	-	-	0.037	0.897	0.066	-	-	7.31	13.6	133.5
	64.3	10.7	0.044	0.933	0.023	-	-	-0.033*	0.945*	0.088*	-	-	5.17*	4.3	41.87
	65.7	12.05	0.044	0.928	0.028	-	-	-0.083*	1.07*	0.014*	-	-	3.15*	1.68	16.27
9**	31.3	2.5	-	0.994	0.004	0.002	-	-	0.893	0.064	0.043	-	5.46	18.5	187.7
	33.6	3.3	-	0.993	0.005	0.002	-	-	0.880	0.071	0.049	-	5.56	16.6	167.4
	35.5	4.15	-	0.992	0.006	0.002	-	-	0.869	0.077	0.054	-	6.21	16.6	166.0
	36.7	4.95	-	0.990	0.008	0.003	-	-	0.862	0.079	0.059	-	5.69	13.9	138.4
	37.8	6.3	-	0.986	0.010	0.004	-	-	0.862	0.078	0.060	-	6.77	15.5	153.4
	39.4	7.7	-	0.982	0.013	0.005	-	-	0.860	0.077	0.064	-	7.40	15.0	147.1
	42.1	9.1	-	0.975	0.019	0.006	-	-	0.847	0.073	0.079	-	6.45	9.58	93.4
	43.4	10.1	-	0.972	0.021	0.008	-	-	0.844	0.072	0.085	-	7.09	8.82	85.4
	45	11.15	-	0.968	0.023	0.009	-	-	0.783*	0.085*	0.131*	-	12.17*	7.87	75.8
10	22.8	2.4	-	0.971	0.017	0.004	0.008	-	0.731	0.107	0.113	0.049	6.60	19.6	198.9
	23.1	3.45	-	0.968	0.019	0.005	0.008	-	0.734	0.105	0.113	0.049	8.05	23.9	241.0
	27.5	7.6	-	0.942	0.035	0.008	0.015	-	0.706	0.102	0.143	0.049	7.09	15.7	157.6
	29.7	9.15	-	0.930	0.041	0.012	0.017	-	0.682	0.101	0.166	0.051	5.54	10.0	99.4
	30.5	9.9	-	0.923	0.044	0.015	0.018	-	0.683	0.098	0.169	0.050	6.13	10.2	100.9
	31.2	10.8	-	0.915	0.046	0.020	0.019	-	0.689	0.096	0.165	0.050	7.56	11.7	115.2

	32.2	11.7	-	0.906	0.048	0.026	0.021	-	0.693	0.095	0.163	0.049	8.69	11.9	115.9
	33.4	12.65	-	0.896	0.050	0.032	0.022	-	0.700	0.094	0.157	0.049	10.20	11.6	112.3
	34.6	13.65	-	0.888	0.052	0.037	0.023	-	0.700	0.093	0.157	0.050	11.11	9.88	95.2
	34.8	14.7	-	0.887	0.052	0.038	0.023	-	0.702	0.091	0.157	0.050	10.97	9.48	90.6
	35.2	15.65	-	0.885	0.053	0.039	0.023	-	0.704	0.089	0.159	0.048	13.66	11.1	105.5
	36.1	16.6	-	0.879	0.054	0.042	0.024	-	0.707	0.085	0.159	0.049	16.23	10.2	96.7
	38.1	17.7	-	0.863	0.057	0.054	0.026	-	0,909*	0,050*	0,008*	0,033*	52.57*	10.8	101.1
	38.2	18.6	-	0.863	0.057	0.054	0.026	-	0,902*	0,052*	0,013*	0,033*	46.08*	7.90	73.5
	21.4	2.75	-	0.955	0.024	0.007	0.014	-	0.728	0.079	0.153	0.040	7.23	22.0	222.6
	21.6	4.3	-	0.955	0.024	0.007	0.014	-	0.726	0.080	0.154	0.040	7.26	22.0	222.0
	21.8	4.85	-	0.953	0.025	0.009	0.014	-	0.726	0.080	0.154	0.040	7.37	22.3	222.8
	22.1	5.9	-	0.951	0.025	0.010	0.014	-	0.724	0.080	0.155	0.041	7.36	22.0	218.8
11	22.6	6.8	-	0.948	0.027	0.011	0.014	-	0.722	0.080	0.157	0.041	7.23	21.1	208.6
	23.6	7.45	-	0.939	0.031	0.015	0.016	-	0.719	0.078	0.162	0.041	7.55	20.8	204.1
	25.3	9.2	-	0.926	0.035	0.022	0.017	-	0.714	0.076	0.169	0.041	7.81	19.2	187.7
	28.2	11.05	-	0.905	0.042	0.032	0.021	-	0.706	0.070	0.184	0.040	8.60	16.6	160.8
	37.2	18.15	-	0.845	0.050	0.078	0.027	-	0,971*	0,040*	-0,012*	-0,001	34*	5.94	57.1



Table 10. Experimental data (Gas 12, low crystallization rate).

\* equilibrium points near total dissociation, hydrate composition errors close to 100%

Gas	P ( $\pm 0.1$ bar)	T ( $\pm 0.2$ $^{\circ}\text{C}$ )	Molar gas fraction ( $\pm 0.001$ )			Molar hydrate fraction ( $\pm 0.003$ )			N <sub>hyd</sub>	water conversion %	Hydrate volume (mL $\pm 4\%$ )
			CO <sub>2</sub>	CH <sub>4</sub>	C <sub>2</sub> H <sub>6</sub>	CO <sub>2</sub>	CH <sub>4</sub>	C <sub>2</sub> H <sub>6</sub>			
	41.7	6.2	0.037	0.943	0.020	0.117*	0.669*	0.214*	35.3*	9.67	98.0
	37.75	4.6	0.035	0.951	0.014	0.081	0.799	0.120	10.3	9.84	99.1
	35.6	4.2	0.034	0.952	0.014	0.081	0.828	0.091	9.61	13.1	131.2
12	31.8	3.25	0.033	0.957	0.010	0.075	0.849	0.076	6.75	13.9	137.4
	30.4	2.45	0.031	0.959	0.010	0.076*	0.854*	0.070*	5.72	13.1*	129.2*
	27.6	1.3	0.030	0.963	0.007	0.075	0.862	0.063	5.83	16.4	160.9
	35.7	4.2	0.037	0.948	0.015	0.062	0.843	0.095	6.92	8.59	83.5

Table 11. Experimental versus predicted results (Gas 1 to 5)  
 \* equilibrium points near total dissociation, hydrate composition errors close to 100%  
 \*\* hydrate composition uncertainties  $\approx 10\%$  for  $C_2H_6$  and  $C_3H_8$

Gas	$P_{exp}$ ( $\pm 0.1$ bar)	T ( $\pm 0.2$ $^{\circ}C$ )	Exp. hydrate composition (mol. frac., $\pm 0.001$ )				struct.	$P_{pred}$ (bar)	Predicted hydrate composition (mol. frac.)		
			N <sub>2</sub>	CO <sub>2</sub>	CH <sub>4</sub>	N <sub>2</sub>			CO <sub>2</sub>	CH <sub>4</sub>	
1	16.2	2.2	-	1	-	S1	16.5	-	-	-	
	18.2	3.3	-	1	-	S1	19.0	-	-	-	
	20.1	4.1	-	1	-	S1	20.5	-	-	-	
	22.6	5	-	1	-	S1	22.8	-	-	-	
						dev. %	2.3				
2	37	3	-	-	1	S1	35.6	-	-	-	
	42	4.5	-	-	1	S1	41.4	-	-	-	
	47.4	5.7	-	-	1	S1	46.8	-	-	-	
	55.4	7.3	-	-	1	S1	55.2	-	-	-	
	64.9	8.8	-	-	1	S1	64.8	-	-	-	
	70.5	9.7	-	-	1	S1	71.4	-	-	-	
					dev. %	1.4					
3	33.3	3.4	-	0.290	0.71	SI	32.9	-	0.227	0.773	
	35.3	4.4	-	0.289	0.711	SI	36.2	-	0.235	0.765	
	37.1	4.9	-	0.288	0.712	SI	38.0	-	0.244	0.756	
	40.3	5.8	-	0.284	0.716	SI	41.4	-	0.256	0.744	
	44.5	6.8	-	0.277	0.723	SI	45.7	-	0.270	0.730	
	49.3	7.8	-	0.259	0.741	SI	50.6	-	0.283	0.717	
	56	9	-	0.232*	0.768*	SI	57.6	-	0.290	0.710	
					dev. %	2.4	-	20.4	37.3		
4	29.1	2.2	-	0.292	0.708	SI	29.3	-	0.219	0.781	
	29.7	2.5	-	0.282	0.718	SI	30.0	-	0.232	0.768	
	31.8	3.6	-	0.283	0.717	SI	33.3	-	0.239	0.761	
	34.7	4.5	-	0.270	0.73	SI	36.3	-	0.254	0.746	
	38	5.2	-	0.227	0.773	SI	38.5	-	0.276	0.724	
	41.6	6.4	-	0.101	0.899	SI	43.4	-	0.288	0.712	
	56.3	9.5	-	-*	-*	SI	-	-	-	-	
					dev. %	2.8	-	45.2	8.800		

	24.6	2.46	0.059	0.941	-	SI	25.3	0.045	0.955	-
	26	2.6	0.067	0.933	-	SI	26.9	0.042	0.958	-
	26.6	2.66	0.073	0.927	-	SI	27.3	0.040	0.960	-
5	28.7	2.87	0.087	0.913	-	SI	29.9	0.037	0.963	-
	31.3	3.13	0.119	0.881	-	SI	32.2	0.034	0.966	-
	33.8	6.75	0.318*	0.682*		SI	34.8	0.032	0.968	-
						dev. %	3.2	54.200	10.800	-

Table 12. Experimental versus predicted results (Gas 7, 8, 12)  
 \* equilibrium points near total dissociation, hydrate composition errors close to 100%  
 \*\* hydrate composition uncertainties  $\approx 10\%$  for  $C_2H_6$  and  $C_3H_8$

Gas	Pexp ( $\pm 0.1$ bar)	T ( $\pm 0.2$ °C)	Exp. hydrate composition (mol. frac.. $\pm 0.001$ )				struct.	Ppred (bar)	Predicted hydrate composition (mol. frac.)			Ppred (bar)	Predicted hydrate composition (mol. frac.)		
			CO2	CH4	C2H6				CO2	CH4	C2H6			CO2	CH4
7**	27.1	1	-	-	-	SI	25.7	-	-	-	SII	21.74	-	-	-
	27.6	1.4	-	-	-	SI	26.6	-	-	-	SII	22.56	-	-	-
	28.3	2	-	-	-	SI	28	-	-	-	SII	23.86	-	-	-
	28.8	2.5	-	-	-	SI	28.8	-	-	-	SII	24.82	-	-	-
	28.9	2.8	-	-	-	SI	29.2	-	-	-	SII	25.36	-	-	-
	29.3	3.3	-	-	-	SI	30.3	-	-	-	SII	26.5	-	-	-
	30.2	4	-	-	-	SI	31.5	-	-	-	SII	27.98	-	-	-
	30.6	5	-	-	-	SI	34.5	-	-	-	SII	30.78	-	-	-
	30.6	5.8	-	-	-	SI	37.5	-	-	-	SII	33.47	-	-	-
						dev. %	6	-	-	-	dev. %	11.9	-	-	-
8	35.4	2.75	0.07	0.888	0.042	S1	31.1	0.046	0.873	0.081	S2	26	0.032	0.919	0.049
	38.1	3.65	0.07	0.888	0.042	S1	33.5	0.051	0.858	0.091	S2	28.2	0.035	0.909	0.056
	42.3	5.15	0.069	0.891	0.041	S1	37.9	0.054	0.835	0.111	S2	32.5	0.038	0.895	0.067
	45.6	6.55	0.07	0.891	0.039	S1	43.3	0.056	0.827	0.117	S2	37.3	0.04	0.89	0.07
	51.2	7.8	0.068	0.889	0.042	S1	47.6	0.058	0.814	0.128	S2	42.2	0.041	0.882	0.077
	59.9	9.25	0.037	0.897	0.066	S1	56.7	0.068	0.816	0.116	S2	49.4	0.049	0.881	0.07
	64.3	10.7	-0.033*	0.945*	0.088*	S1	66.6	0.069	0.812	0.118	S2	57.7	0.05	0.878	0.073
	65.7	12.05	-0.083*	1.07*	0.014*	S1	76.1	0.067	0.801	0.133	S2	66.4	0.048	0.871	0.08
					dev. %	8.9	33.6	6.0	143	dev. %	17.5	44	1.5	47	
12	41.7	6.2	0.117*	0.669*	0.214*	S1	41.2	0.062	0.811	0.127	S2	35.7	0.044	0.88	0.076
	37.75	4.6	0.081	0.799	0.12	S1	36.4	0.062	0.843	0.095	S2	31	0.044	0.898	0.058
	35.6	4.2	0.081	0.828	0.091	S1	35.1	0.061	0.846	0.093	S2	29.8	0.043	0.901	0.056
	31.8	3.25	0.075	0.849	0.076	S1	32.8	0.061	0.869	0.07	S2	27.5	0.042	0.915	0.043

---

30.4	2.45	0.076*	0.854*	0.070*	S1	30.3	0.059	0.871	0.07	S2	25.4	0.04	0.917	0.043
27.6	1.3	0.075	0.862	0.063	S1	27.5	0.057	0.885	0.058	S2	22.8	0.039	0.926	0.035
35.7	4.2	0.062	0.843	0.095	S1	34.7	0.066	0.835	0.099	S2	29.7	0.046	0.894	0.06
					dev. %	1.8	23.8	5.3	12	dev. %	16.1	45.7	11.6	45.4

---

